BIOCHEMISTRY
including biophysical chemistry & molecular biology

Article

pubs.acs.org/biochemistry

Probing the Redox States of Sodium Channel Cysteines at the Binding Site of μO§-Conotoxin GVIIJ

Min-Min Zhang,[†] Joanna Gajewiak,[†] Layla Azam,[†] Grzegorz Bulaj,[‡] Baldomero M. Olivera,[†] and Doju Yoshikami*,[†]

[†]Department of Biology, University of Utah, Salt Lake City, Utah 84112, United States

[‡]Department of Medicinal Chemistry, College of Pharmacy, University of Utah, Salt Lake City, Utah 84108, United States

Supporting Information

ABSTRACT: μO§-Conotoxin GVIIJ is a 35-amino acid peptide that readily blocks six of eight tested Na_V1 subunit isoforms of voltage-gated sodium channels. μO§-GVIIJ is unusual in having an S-cysteinylated cysteine (at residue 24). A proposed reaction scheme involves the peptide−channel complex stabilized by a disulfide bond formed via thiol−disulfide exchange between Cys24 of the peptide and a Cys residue at neurotoxin receptor site 8 in the pore module of the channel (specifically, Cys910 of rat $Na_V1.2$). To examine this model, we synthesized seven derivatives of μO§-GVIIJ in which Cys24 was disulfide-bonded to various thiols (or SR groups) and tested them on voltage-clamped *Xenopus laevis* oocytes expressing $Na_V1.2$. In the proposed model, the SR moiety is a leaving group that is no longer present in the final peptide−channel complex; thus, the same k_{off} value should be obtained regardless of the SR group. We observed that all seven derivatives, whose k_{on} values varied over a 30-fold range, had the same k_{off} value. Concordant results were observed with $Na_V1.6$, for which the k_{off} was 17-fold larger. Additionally, we tested two μO§-GVIIJ derivatives (where SR was glutathione or a free thiol) on two $Na_V1.2$ Cys replacement mutants ($Na_V1.2$[C912A] and $Na_V1.2$[C918A]) without and with reduction of channel disulfides by dithiothreitol. The results indicate that Cys910 in wild-type $Na_V1.2$ has a free thiol and conversely suggest that in $Na_V1.2$[C912A] and $Na_V1.2$[C918A], Cys910 is disulfide-bonded to Cys918 and Cys912, respectively. Redox states of extracellular cysteines of sodium channels have hitherto received scant attention, and further experiments with GVIIJ may help fill this void.

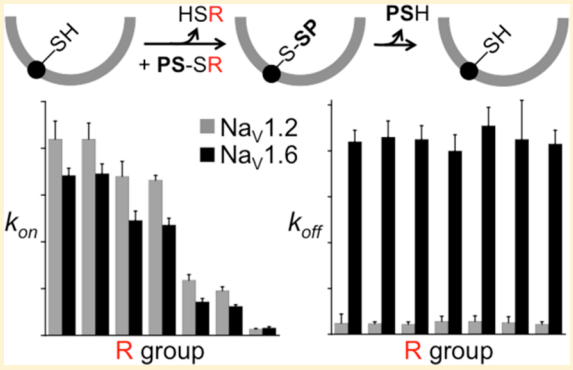

Voltage-gated sodium channels (VGSCs) play a critical role in action potentials of excitable tissue. Each VGSC consists of a large α-subunit (of which there are nine isoforms, $Na_V1.1$−1.9) associated with one or two much smaller β-subunits (of which there are four isoforms, $Na_Vβ1$−$β4$).[1,2] The α-subunit has four homologous domains (DI−DIV), each composed of six transmembrane-spanning segments (S1−S6), where S1−S4 comprise the voltage sensor module and S5 and S6 comprise the pore module, and the extracellular loop connecting S5 and S6 has a membrane reentrant pore loop with two segments, SS1 and SS2, in the middle (see Figure 1B). The four pore modules are radially arranged with the reentrant loops lining the central Na^+-selective conductance pore, and this core of pore modules is surrounded by the voltage sensor modules.[1] The β-subunit consists of a single transmembrane-spanning segment and modulates the activity, expression, and localization of VGSCs.[3,4]

Aspects of VGSCs that have received scant attention are the functions and oxidation states of the extracellular cysteine residues, largely because there has been no facile means of probing them. The different Na_V1 isoforms have approximately a dozen such Cys residues, all located in the vicinity of pore loops (Figure 1B). Of these extracellular cysteines, the redox states of only three are known. One is in the pore loop of DI exclusively of $Na_V1.5$ and has a free thiol as judged by its reactivity with methanethiosulfonate analogues that block Na^+ conductance.[5] The second, whose location remains to be definitively established, has a free thiol that allows maleimide conjugates of saxitoxin to irreversibly block $Na_V1.4$.[6] The third is involved in disulfide bond formation with subunit β2 or β4; although the Cys residue in the Na_V β-subunit that participates in the disulfide bond is known,[7,8] its opposite number in the α-subunit remains to be established, although possibilities have been suggested.[7] The redox state of a fourth cysteine (which may be the same as the third, just discussed, cysteine) has been suggested in view of its putative reaction with the recently discovered μO§-conotoxin GVIIJ (abbreviated GVIIJ), as described below and in Discussion.

GVIIJ is a VGSC blocker with an unusual structure and novel binding site on the channel; some salient features of this

Received: April 13, 2015
Revised: June 2, 2015
Published: June 3, 2015

DOI: 10.1021/acs.biochem.5b00390
Biochemistry 2015, 54, 3911−3920

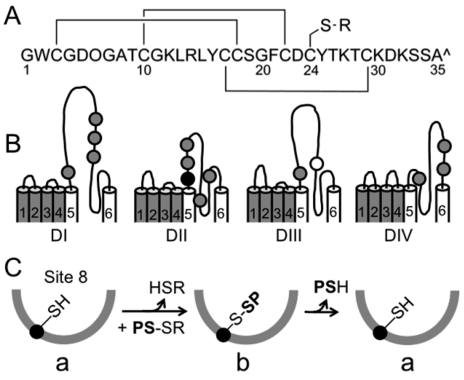

Figure 1. μO§-Conotoxin GVIIJ, its sodium channel target, and the proposed reaction between the two. (A) Sequence of synthetic $GVIIJ_{SSR}$, where the subscripted SR refers to the group disulfide bonded to Cys24 of the peptide backbone. (See Table 2 for structures of SR groups use in this report.) O and ^ signify hydroxyproline and a free C-terminal carboxyl, respectively (after ref 9). (B) Part of transmembrane segments and their extracellular connecting loops of the α-subunit of VGSCs (after ref 25). The four domains are labeled DI–DIV. Transmembrane segments of the voltage sensor modules are represented as dark cylinders (S1–S4), and those of the pore modules are white cylinders (S5 and S6). Circles indicate approximate locations of the extracellular Cys residues of GVIIJ-sensitive channels from rat and human. The first Cys in DII (●) is the location of Cys910 of $rNa_V1.2$. $rNa_V1.4$ has a Ser instead of Cys at the empty circle in DIII. Aligned sequences of residues in the S5–S6 loops of DI–DIV of rat and human $Na_V1.1$–1.9 are provided in Table S1 of the Supporting Information. (C) Proposed disulfide-exchanged reaction between $GVIIJ_{SSR}$ and the Cys at site 8 (Cys910 in the case of $rNa_V1.2$). PS represents the peptide backbone of GVIIJ, and SR represents the moiety disulfide-bonded to Cys24 of the peptide.

peptide taken from ref 9 are briefly reviewed here. GVIIJ has seven Cys residues in the peptide backbone, six of which are disulfide-bonded to each other; the seventh cysteine, Cys24, is S-cysteinylated (Figure 1A). When Cys24 is disulfide-bonded to cysteine or glutathione (abbreviated $GVIIJ_{SSC}$ or $GVIIJ_{SSG}$, respectively), the block reverses very slowly; in contrast, the block is readily reversible when Cys24 has a free thiol (abbreviated $GVIIJ_{SH}$). Eight rat Na_V1 isoforms ($rNa_V1.1$–1.8) and seven human isoforms ($hNa_V1.1$–1.7) exogenously expressed in oocytes and mammalian cell lines, respectively, were tested with synthetic $GVIIJ_{SSG}$, and all were readily blocked except $rNa_V1.5$, $hNa_V1.5$, and $rNa_V1.8$. A common feature of the susceptible channels is the presence of three Cys residues in the link between S5 and SS1 in DII (Figure 1B); in $rNa_V1.2$, they are Cys910, Cys912, and Cys918. None of these three Cys residues is present at homologous locations in rat and human $Na_V1.5$, $Na_V1.8$, or $Na_V1.9$ (Table S1 of the Supporting Information). Chimeras of $hNa_V1.5$ and $hNa_V1.7$ where their DII residues were swapped had sensitivities that were the reciprocals of those of $GVIIJ_{SSG}$. The mutant $rNa_V1.2$[C910L] was significantly less sensitive to $GVIIJ_{SSG}$; conversely, $rNa_V1.5$[L869C] was readily blocked by $GVIIJ_{SSG}$. [Note, Leu869 of $rNa_V1.5$ is at a location homologous to that of Cys910 of $rNa_V1.2$ (see Table S1 of the Supporting Information).]

These results pinpointed Cys910 of $rNa_V1.2$ (black circle in Figure 1B) as a critical residue and defined GVIIJ's binding site as site 8. Competition experiments[9] further demonstrated that site 8 is distinct from the binding sites of two other conotoxins that block VGSCs, μ-conotoxins and μO-conotoxins. μ-Conotoxins, like tetrodotoxin, target the sodium-conducting pore of the channel (or site 1),[10] while μO-conotoxins target the extracellular loop between S3 and S4 of DII (or site 4).[11]

Results of treatment of oocytes with the sulfhydryl reducing and oxidizing agents, dithiothreitol (DTT) and Cu^{2+}-phenanthrolene, respectively, suggested that the oxidation state of $rNa_V1.2$'s Cys910 was critical for the binding of $GVIIJ_{SSG}$, and it was hypothesized that a disulfide bond could form between Cys24 of $GVIIJ_{SSG}$ (or $GVIIJ_{SSC}$) and Cys910 of $rNa_V1.2$ by a disulfide-exchange mechanism whereby the SR group disulfide-bonded to Cys24 (Figure 1A) would be a leaving group and therefore absent from the final toxin–channel complex (Figure 1C).[9] In the first part of this report, we compare the activities of seven $GVIIJ_{SSR}$ derivatives (all identical except for the SR group) on $rNa_V1.2$ and, for comparison, $Na_V1.6$ from mouse ($mNa_V1.6$). To help explain the reversibility of the block by $GVIIJ_{SSR}$, we examined the sodium currents of channels where thiocholine was disulfide-bonded to the sulfhydryl of a cysteine residue at site 1 in the pore loop of DI of $rNa_V1.5$ and $rNa_V1.2$[F385C] (see Table S1 of the Supporting Information); both disulfide bonds proved to be labile, like the proposed disulfide bond between GVIIJ and the Cys residue at site 8 of the channel (Figure 1C). In the second part of this report, we explore the possible contributions of residues Cys912 and Cys918 of $rNa_V1.2$ by examining the cysteine replacement channel mutants $rNa_V1.2$[C912A] and $rNa_V1.2$[C918A].

MATERIALS AND METHODS

Peptide Syntheses. The primary structure of GVIIJ is illustrated in Figure 1A. In the native peptide, Trp2 is brominated and the SR group disulfide-bonded to Cys24 is a cysteine. Synthetic GVIIJ (i.e., $GVIIJ_{SSC}$) with and without bromination of Trp2 blocked $rNa_V1.2$ with respective k_{on} and k_{off} values that differed by a factor of <2 (Table S3 of ref 9); in view of this similarity in functional activity and to minimize the cost of starting materials, all GVIIJ derivatives in this report were synthesized with nonbrominated Trp2. In all, eight GVIIJ derivatives were tested; all had the same peptide backbone and differed from each other by how the sulfur of Cys24 of GVIIJ's backbone was modified. In the $GVIIJ_{SH}$ derivative, Cys24 had a free thiol, while in the $GVIIJ_{SSR}$ derivatives, Cys24 was disulfide-bonded to various SR groups. The syntheses of the linear GVIIJ as well as its fully oxidatively folded derivatives, $GVIIJ_{SH}$, $GVIIJ_{SSG}$, and $GVIIJ_{SSC}$, were previously described.[9] Here we present the syntheses of the five remaining derivatives and their structural characterization.

$GVIIJ_{SSEA}$ was obtained by oxidative folding in the presence of cystamine dihydrochloride. One hundred nanomoles of linear GVIIJ was suspended in 0.5 mL of a 0.01% TFA (Fisher BioReagents, Fair Lawn, NJ) solution and added to a solution containing 2.5 mL of 0.2 M Tris-HCl (pH 7.5) (Sigma-Aldrich, St. Louis, MO) and 0.2 mM EDTA (Mallinckrodt, Paris, KY), 1 mL of 10 mM cystamine dihydrochloride (ICN Biomedicals Inc., Aurora, OH) dissolved in water, and 1.5 mL of water. The oxidation was also conducted under the same general conditions but with 0.5 mL of the cystamine dihydrochloride solution. The final peptide concentration in the folding mixture was 20 μM. The folding reaction was conducted for 22 h at room temperature (~22 °C) and quenched with formic acid so its final concentration was 8%. The quenched reaction mixture was fractionated by reversed phase high-performance liquid chromatography (HPLC) using a semipreparative Vydac C_{18}

DOI: 10.1021/acs.biochem.5b00390
Biochemistry 2015, 54, 3911–3920

Table 1. HPLC Retention Times, Purities, and Molecular Masses of Five Synthetic GVIIJ$_{SSR}$ Derivatives

peptide	SR group[a]	HPLC RT (min)[b]	purity (%)	$[M + H]^+$ predicted (Da)	$[M + H]^+$ observed (Da)
GVIIJ$_{SSEA}$	-S$(CH_2)_2NH_3^+$	18.475	>97[c]	3812.5221	3812.1806[d]
GVIIJ$_{SSET}$	-S$(CH_2)_2N(CH_3)_3^+$	18.502	>96[c]	3854.5691[e]	3854.5567[e,f]
GVIIJ$_{SSMe}$	-SCH_3	19.208	98	3783.4955	3783.3692[d]
GVIIJ$_{SSES}$	-S$(CH_2)_2SO_3^-$	19.435	99	3877.4680	3877.5369[d]
$(GVIIJ_S)_2$[g]	GVIIJ$_{s-}$	22.195	>95[c]	7473.0000	7473.0575[f]

[a]Chemical names of SR groups: SEA, 2-aminoethanethiol (also known as cysteamine); SET, (2-mercaptoethyl)trimethylammonium (also known as thiocholine); SMe, thiomethyl; SC, cysteine; SES, 2-mercaptoethanesulfonic acid. [b]Retention time (RT) of the HPLC peak in Figure 2A, with respect to the start of the run. [c]Syntheses of GVIIJ$_{SSEA}$, GVIIJ$_{SSET}$, and $(GVIIJ_S)_2$ were performed on different occasions throughout the study, and the purities of these analogues were at least those indicated here. [d]MALDI mass spectrometry. [e]Predicted and observed masses of GVIIJ$_{SSET}$ are for $[M]^+$. [f]ESI mass spectrometry. [g]Peptide dimer in which the monomeric units are disulfide-linked through Cys24.

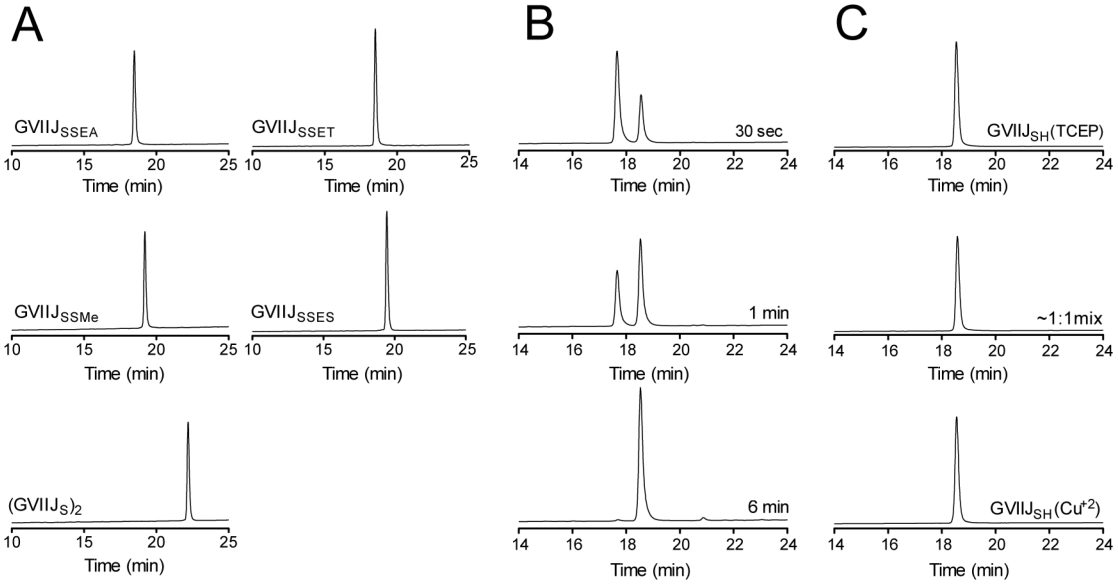

Figure 2. HPLC elution profiles of (A) five synthetic GVIIJ$_{SSR}$ derivatives, (B) products of TCEP reduction of GVIIJ$_{SSEA}$ at three reaction times, and (C) the major reaction product produced by TCEP reduction of GVIIJ$_{SSEA}$ compared with GVIIJ$_{SH}$ itself. HPLC was performed on analytical C18 columns as described in Materials and Methods. (A) Structures of the SR groups disulfide-bonded to Cys24 of the peptides are listed in Table 1 along with peptide retention times, purities, and molecular masses. Mass spectra of these peptides are provided in the Supporting Information. (B) TCEP reduction products of GVIIJ$_{SSEA}$ after 30 s, 1 min, and 6 min (top, middle, and bottom panels, respectively). The TCEP reaction was conducted as described in Materials and Methods. (C) Major product resulting from TCEP reduction of GVIIJ$_{SSEA}$ (top), GVIIJ$_{SH}$ synthesized by Cu^{2+}-catalyzed folding of the linear peptide[9] (bottom), and an ~1:1 mixture of the two (middle). The single co-eluting peak in the middle panel indicates that the major product produced by TCEP reduction of GVIIJ$_{SSEA}$ was GVIIJ$_{SH}$.

column (218TP510, 250 mm × 10 mm, 5 μm particle size) (Grace, Deerfield, IL). The column was eluted with a linear gradient ranging from 15 to 45% solvent B over 30 min at a flow rate of 4 mL/min. The HPLC solvents were 0.1% (v/v) TFA in water (solvent A) and 0.1% TFA (v/v) in 90% aqueous acetonitrile (solvent B). The eluent was monitored by absorbance at 220 and 280 nm. The purity of the folded peptide was assessed on an analytical C_{18} Vydac column (218TP54, 250 mm × 4.6 mm, 5 μm particle size) (Grace) using the gradient described above, with a flow rate of 1 mL/min. Purified GVIIJ$_{SSEA}$ was quantified by absorbance at 280 nm using an extinction coefficient (ε) value of 8480 M^{-1} cm^{-1}. On average, 24 nmol of GVIIJ$_{SSEA}$ was obtained from 100 nmol of linear peptide in the folding reaction. The molecular mass of GVIIJ$_{SSEA}$ was confirmed by MALDI MS (Table 1), and its HPLC elution profile is shown in Figure 2A; the retention time of the peak is reported in Table 1. To confirm that GVIIJ$_{SSEA}$ had a peptide backbone with the correct disulfide bonding pattern, it was reduced with Pierce's tris(2-carboxyethyl)-phosphine hydrochloride (TCEP) (Thermo Fisher Scientific, Waltham, MA). A solution of 4 nmol of GVIIJ$_{SSEA}$ in 20 μL of 0.1% TFA was treated with 20 μL of 30 mM TCEP in sodium citrate buffer (pH 3) at room temperature. HPLC analysis showed that a single major product progressively accumulated with time (Figure 2B), which co-eluted with GVIIJ$_{SH}$ (Figure 2C) whose disulfide bonding pattern was previously established.[9]

GVIIJ$_{SSET}$, GVIIJ$_{SSES}$, and GVIIJ$_{SSMe}$ were obtained by reacting GVIIJ$_{SH}$ with the appropriate methanethiosulfonate (MTS) derivative (or MTS-SR reagent). (MTS-SR reagents specifically add the SR moiety to reduced thiols to form mixed disulfides.[12,13]) To produce these peptides, GVIIJ$_{SH}$ was suspended in either 0.01% TFA or a mixture of the HPLC solvents and reacted with a large excess of MTS-SR reagent, either 2-(trimethylammonium)ethylmethanethiosulfonate (Anatrace, Maumee, OH), 2-sulfonatoethylmethanethiosulfonate (Affymetrix, Cleveland, OH), or *S*-methylmethanethiosulfonate (Sigma-Aldrich), to yield GVIIJ$_{SSET}$, GVIIJ$_{SSES}$, or GVIIJ$_{SSMe}$, respectively. The final peptide concentration in the folding mixture varied between 7.5 and 43 μM. The reaction

DOI: 10.1021/acs.biochem.5b00390
Biochemistry 2015, 54, 3911−3920

was conducted for 20−45 min at room temperature and then the mixture diluted with solvent A before being purified by HPLC as described above for $GVIIJ_{SSEA}$. Purified derivatives were quantified by absorbance at 280 nm as described for $GVIIJ_{SSEA}$. The yield of the reactions ranged from 52 to 75%. The molecular masses of the analogues were confirmed by MALDI MS and ESI MS (Table 1). The HPLC elution profiles of the peptides are shown in Figure 2, and the retention times of the peaks are listed in Table 1. This method was also used as an additional way to confirm the disulfide bonding pattern of $GVIIJ_{SSEA}$. An excess of 2-aminoethylmethanethiosulfonate hydrobromide (Anatrace) was reacted with $GVIIJ_{SH}$ for 15 min at room temperature. The product was purified by C18 analytical HPLC, and it co-eluted with $GVIIJ_{SSEA}$ obtained from the linear peptide using the protocol described above (data not shown).

Formation of the $(GVIIJ_S)_2$ dimer was achieved by DMSO-assisted oxidation[14] of $GVIIJ_{SH}$. Sixty nanomoles of $GVIIJ_{SH}$ was dissolved in 0.24 mL of 0.01% TFA and 0.72 mL of 0.2 M Tris-HCl (pH 7.5) with 0.2 mM EDTA. The reaction mixture was vortexed, and 0.24 mL of DMSO (EMD Millipore, Darmstadt, Germany) was added. The reaction was allowed to proceed for 19 h at room temperature and the mixture diluted with solvent A before being purified. Peptide was purified by HPLC as described above for $GVIIJ_{SSEA}$. Purified $(GVIIJ_S)_2$ dimer was quantified by measuring the absorbance at 280 nm using an ε value of 16960 M^{-1} cm^{-1} (i.e., double that of the monomeric GVIIJ derivatives). On average, 17 nmol of $(GVIIJ_S)_2$ was obtained from 60 nmol of $GVIIJ_{SH}$ in the dimerization reaction for a 57% yield. The molecular mass of $(GVIIJ_S)_2$ was confirmed by ESI MS (Table 1). The HPLC elution profile of the peptide is shown in Figure 2, and the retention time of the peak is reported in Table 1. [The dimer could also be obtained in one step from the linear peptide via Cu^{2+}-catalyzed air oxidation normally used to obtain $GVIIJ_{SH}$[9] by increasing the time or the temperature of the reaction (not illustrated).]

Preparation of cRNAs. Clones of rat $Na_V1.2$ (NM_012647), rat $Na_V1.5$ (NM_013125), and mouse $Na_V1.6$ (NM_011323) were obtained from A. Goldin (University of California, Irvine, CA). The clone for $rNa_V1.2$-[F385C] was prepared as previously described.[15] The clones for $rNa_V1.2$[C912A] and $rNa_V1.2$[C918A] were prepared as follows. Primers with the desired mutation (for both mutants, a change from TGT to GCC) flanked by 18−21 bases on each side were designed. The mutations were introduced by polymerase chain reaction (PCR) using either *Pfu* Turbo (Agilent, Santa Clara, CA) or Phusion (Thermo Fisher Scientific) DNA polymerase. The template DNA was subsequently digested by restriction enzyme DpnI. The PCR products were transformed into DH10B competent cells and plated on tetracycline resistant LB Agar plates and incubated overnight at 37 °C. The following day, inoculated LB plus tetracycline cultures were grown overnight at 37 °C. The DNA was isolated using Qiaprep spin columns (Qiagen, Valencia, CA) and sequenced to confirm the presence of the mutations. The mutated cDNAs were linearized with NotI, and cRNA was transcribed with T7 RNA polymerase using the Ambion mMessage mMachine RNA polymerase kit (Life Technologies, Carlsbad, CA). The concentration of the cRNA was determined by UV spectroscopy.

Preparation of *Xenopus laevis* Oocytes and Injection of cRNA into Them. Oocytes were harvested and prepared essentially as previously described.[16] Briefly, freshly excised oocytes were treated with 2.5 mg/mL collagenase A (Roche Diagnostics) in OR-2 [82.5 mM NaCl, 2.0 mM KCl, 1.0 mM $MgCl_2$, and 5 mM Hepes (pH 7.3)] for 1−2 h on a rotary shaker at room temperature. Halfway through the treatment, the solution was exchanged with a fresh collagenase solution. The oocytes were then rinsed with OR-2 and incubated until they were used at 16 °C in ND96 [96 mM NaCl, 2 mM KCl, 1.8 mM $CaCl_2$, 1 mM $MgCl_2$, and 5 mM Hepes (pH 7.3)] supplemented with penicillin (100 units/mL) and streptomycin (0.1 mg/mL). Use of *X. laevis* frogs, which provided oocytes for this study, followed protocols approved by the University of Utah Institutional Animal Care and Use Committee that conform to the National Institutes of Health Guide for the Care and Use of Laboratory Animals.

$Na_V1.6$ cRNA from mouse, rather than that from rat, was used in these experiments because much better expression of Na currents was obtained with the former. Injections of $rNa_V1.2$ and $mNa_V1.6$ cRNA into oocytes were conducted as previously described.[17,18] Briefly, a given oocyte was injected with 30−50 nL of distilled water containing 1.5 or 10 ng of cRNA for $rNa_V1.2$ or $mNa_V1.6$, respectively. Oocytes were incubated at 16 °C for 1−3 days in ND96 supplemented with the antibiotics described above.

Two-Electrode Voltage Clamp of Oocytes. This was performed essentially as described previously.[18] The recording chamber consisted of a 4 mm diameter, 30 μL well whose walls and floor consisted of Sylgard (Dow Corning, Midland, MI). Intracellular electrodes contained 3 M KCl (<0.3 MΩ resistances). Sodium currents (I_{Na}) were elicited by stepping the membrane potential to −10 mV, unless indicated otherwise, for 50 ms from a holding potential of −80 mV once every 20 s. Currents were low-pass-filtered at 2 kHz, sampled at a rate of 10 kHz, and leak-subtracted using a P/8 protocol. Data acquisition and analysis were performed with in-house software constructed with LabVIEW (National Instruments, Austin, TX).

Toxin Application. Conopeptides were dissolved in ND96, and we exposed the oocytes to toxin by applying 3 μL of a peptide solution (at 10 times the final concentration) to a static bath with a pipettor and manually stirring the bath for a few seconds by gently aspirating and expelling a few microliters of bath fluid approximately a dozen times with the pipettor. A static bath was used to conserve peptide. Peptides were washed out by continuous perfusion with ND96, initially at a rate of 1.5 mL/min for 20 s and then at a steady rate of 0.5 mL/min. Voltage clamp experiments were conducted at room temperature (~23 °C).

Bovine serum albumin (BSA) is frequently used as a carrier to minimize nonspecific binding of peptides. BSA does not acutely affect the activity of $GVIIJ_{SSG}$.[19] In contrast, $GVIIJ_{SH}$ is affected by BSA in that formation of dimer is observed upon storage of the peptide in saline with 0.1% BSA at 4 °C (data not shown). Thus, we chose to omit BSA altogether.

MTSET Application. Oocytes were treated with MTSET as previously described,[9] which entailed using essentially the same protocol that was used for the toxins described above. MTSET was freshly dissolved in ND96 and used within 1 or 2 min.

Treatment of Oocytes with Dithiothreitol (DTT). This was conducted essentially as previously described;[9] briefly, oocytes were exposed to 2 mM DTT in ND96 for 2 h in 35 mm diameter plastic culture dishes at room temperature (~23

DOI: 10.1021/acs.biochem.5b00390
Biochemistry 2015, 54, 3911−3920

°C) before being rinsed with ND96 and then transferred to the recording chamber.

Data Analysis. Peaks of I_{Na} were monitored before and during exposure to toxin (or MTSET) and its subsequent washout. The time courses of the onset of, and recovery from, block by toxin were fit to single-exponential functions with Prism (GraphPad Software, La Jolla, CA) or KaleidaGraph (Synergy Software, Reading, PA) to obtain k_{obs} and k_{off} values, respectively. Although the putative reaction mechanism involves two steps with the toxin modified in the process (Figure 1C), throughout the reaction the concentrations of toxin and modified toxin remain essentially constant (at the initial toxin concentration and zero, respectively). Therefore, the equation[20]

$$k_{obs} = k_{on}[\text{toxin}] + k_{off}$$

was used, and values of k_{on} were obtained from linear regression fits of k_{obs} versus toxin concentration plots.[21] Values of k_{off} were determined by fitting the toxin-washout curves to a single-exponential function; however, when recovery from block was very slow [<50% recovery after 20 min; i.e., $k_{off} < 0.035$ min^{-1}, as was the case with rNa$_V$1.2 (see Results)], k_{off} was estimated from the level of recovery observed after washing for 20 min and assuming recovery followed a single-exponential time course. (The latter method was also used to determine the k_{off} for the slow recovery from MTSET block during washout of the reagent.) Times longer than 20 min were not used to avoid error caused by possible baseline drift. [In principle, k_{off} values of toxins could also be obtained from the y-intercepts of such plots; however, the magnitudes of the error values were greater than or equal to the mean values themselves, as was experienced previously with μ- and μO-conotoxins (e.g., refs 21−23).] Statistical comparisons were made with two-tailed unpaired t tests. All data are presented as means ± the standard deviation (SD), with N values representing the number of oocytes tested.

RESULTS

Syntheses and Structural Characterization of GVIIJ Derivatives. A total of eight synthetic derivatives of GVIIJ were employed in this report, of which three, GVIIJ$_{SSG}$, GVIIJ$_{SSC}$, and GVIIJ$_{SH}$, were previously described.[9] The syntheses and structural characterization of the five remaining derivatives are detailed in Materials and Methods. Three of these derivatives, GVIIJ$_{SSET}$, GVIIJ$_{SSES}$, and GVIIJ$_{SSMe}$, were prepared from already-folded GVIIJ$_{SH}$ by reaction with commercially available MTS-SR reagents. GVIIJ$_{SH}$ was also used as a starting material to generate the dimer, (GVIIJ$_S$)$_2$, in which the intermolecular disulfide bridge was formed via DMSO-assisted oxidation. To generate GVIIJ$_{SSEA}$, the linear GVIIJ peptide was oxidized in the presence of cystamine. The HPLC elution profiles of these five derivatives are illustrated in Figure 2A; their purities and molecular masses are listed in Table 1, and their mass spectra are presented in the Supporting Information. Experiments to demonstrate that the GVIIJ$_{SSR}$ derivatives had a peptide backbone with the identical disulfide bonding pattern were performed as described in Materials and Methods, and the results are illustrated for GVIIJ$_{SSEA}$ in panels B and C of Figure 2.

Kinetics of Block of rNa$_V$1.2 and mNa$_V$1.6 by GVIIJ$_{SSR}$ Derivatives with Different SR Groups. Much of our previous work with GVIIJ was done with rNa$_V$1.2,[9] so we continued to use this rNa$_V$1 isoform for the experiments described here. Four other rNa$_V$1 isoforms that were susceptible to GVIIJ$_{SSG}$ (i.e., rNa$_V$1.1, rNa$_V$1.3, rNa$_V$1.4, and rNa$_V$1.7) were blocked by GVIIJ$_{SSG}$ with kinetics much like that of rNa$_V$1.2; however, the k_{off} for the block of rNa$_V$1.6 by GVIIJ$_{SSG}$ was significantly larger than those of the other rNa$_V$1 isoforms.[9] The unusually large k_{off} for GVIIJ$_{SSG}$ was also observed for mouse Na$_V$1.6 (mNa$_V$1.6),[19] and because mNa$_V$1.6 was expressed much better in oocytes than rNa$_V$1.6 was, we used mNa$_V$1.6 for comparison with rNa$_V$1.2 in this report. Although GVIIJ$_{SSC}$ more closely resembles the native GVIIJ (Figure 1A), for historical reasons, many more experiments have been conducted with GVIIJ$_{SSG}$ than with GVIIJ$_{SSC}$,[9] so GVIIJ$_{SSG}$ was principally used in experiments for this report.

Representative current traces of rNa$_V$1.2 and mNa$_V$1.6 before and during exposure to GVIIJ$_{SSG}$ are presented in Figure 3A, and sample plots of the time course of toxin block and recovery are illustrated in Figure 3B. The onset of block was used to obtain the observed on-rate constant (k_{obs}) values, while the toxin-washout curves were used to obtain k_{off} values, as described in Materials and Methods. Finally, k_{obs} values were plotted as a function of peptide concentration (Figure 3C),

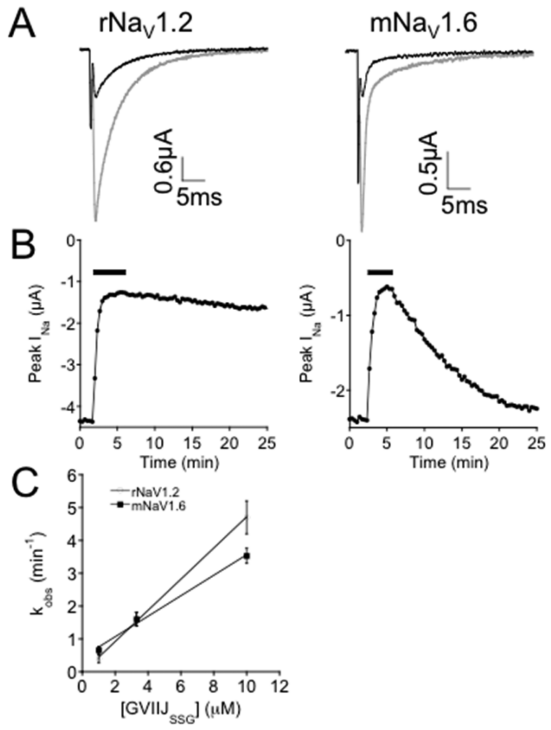

Figure 3. Representative results of block by GVIIJ$_{SSG}$ of rNa$_V$1.2 and mNa$_V$1.6. Oocytes were voltage-clamped at −80 mV, and Na currents were elicited by a voltage step to −10 mV every 20 s as described in Materials and Methods. (A) Traces from oocytes expressing rNa$_V$1.2 (left) and mNa$_V$1.6 (right) before (gray trace) and during (black trace) exposure to 3.3 μM GVIIJ$_{SSG}$. (B) Time course of peak amplitudes of responses of rNa$_V$1.2 (left) and mNa$_V$1.6 (right) before and during exposure to 3.3 μM GVIIJ$_{SSG}$ (black bar) and subsequent washing. Recovery from toxin block of Na$_V$1.6 was much faster than that of Na$_V$1.2. (C) Sample k_{obs} vs GVIIJ$_{SSG}$ concentration plots for rNa$_V$1.2 and mNa$_V$1.6 (○ and ●, respectively). Data points are means ± SD ($N \geq 3$ oocytes per point). Slopes of the plots yielded k_{on} values (see Materials and Methods). Values of k_{on} and k_{off} from replicate trials with GVIIJ$_{SSG}$ and six other SSR derivatives are listed in Table 2 and illustrated in Figure 4.

DOI: 10.1021/acs.biochem.5b00390
Biochemistry 2015, 54, 3911−3920

Table 2. Kinetic Constants for the Block of $rNa_V1.2$ and $mNa_V1.6$ by Seven μO§-$GVIIJ_{SSR}$ Derivatives with Different SR Groups Disulfide-Bonded to Cys24[a]

		$rNa_V1.2$		$mNa_V1.6$	
peptide	SR group	k_{on} (μM^{-1} min^{-1})	k_{off} (min^{-1})	k_{on} (μM^{-1} min^{-1})	k_{off} (min^{-1})
$GVIIJ_{SSEA}$	$-S(CH_2)_2NH_3^+$	2.1 ± 0.19	0.0049 ± 0.0039	1.71 ± 0.077	0.084 ± 0.005
$GVIIJ_{SSET}$	$-S(CH_2)_2N(CH_3)_3^+$	2.1 ± 0.17	0.0047 ± 0.0008	1.73 ± 0.103	0.086 ± 0.007
$GVIIJ_{SSMe}$	$-SCH_3$	1.7 ± 0.16	0.0044 ± 0.001	1.23 ± 0.099[b]	0.085 ± 0.006
$GVIIJ_{SSC}$	$-SCH_2CH(NH_3^+)CO_2^-$	1.66 ± 0.05[c]	0.0057 ± 0.0022[c]	1.18 ± 0.072	0.080 ± 0.007
$GVIIJ_{SSES}$	$-S(CH_2)_2SO_3^-$	0.59 ± 0.06[b]	0.0057 ± 0.0023	0.36 ± 0.035[b]	0.091 ± 0.008
$GVIIJ_{SSG}$	-*S*-glutathione	0.48 ± 0.04[c]	0.0051 ± 0.0026[c]	0.31 ± 0.018	0.085 ± 0.017
$(GVIIJ_S)_2$[d]	$GVIIJ_{s-}$	0.068 ± 0.005[b]	0.0044 ± 0.0011	0.08 ± 0.012[b]	0.083 ± 0.006

[a]Values are mean ± the standard deviation ($n \geq 3$), obtained as described in Materials and Methods. Peptides are listed essentially in descending order of their k_{on} values. [b]The value of k_{on} is significantly different from that immediately above it ($p < 0.05$). [c]Values from Table S3 of ref 9. [d]Peptide dimer in which the monomeric units are disulfide-linked through Cys24. For a given Na_V1 isoform, values of k_{off} for all seven peptides were not significantly different from one another ($p > 0.05$).

from whose slope k_{on} was obtained as described in Materials and Methods.

Seven μO§-$GVIIJ_{SSR}$ derivatives with SR groups with net electrical charges ranging from −1 to +4 and masses from 47 to 3735 Da were examined in the fashion described in the preceding paragraph. The largest derivative was a dimer of μO§-GVIIJ, where one monomer's Cys24 was disulfide-bonded to Cys24 in the other monomer. The structures of the SR groups are illustrated in Table 2, along with the k_{on} and k_{off} values for each derivative in blocking $rNa_V1.2$ and $mNa_V1.6$. The k_{on} values for the different derivatives varied over a range of 20−30-fold, with the k_{on} for a given derivative slightly larger for $rNa_V1.2$ than for $mNa_V1.6$ (except for the dimer, where the reverse was true). In stark contrast, the k_{off} values for all seven derivatives were the same for $rNa_V1.2$ and likewise for $mNa_V1.6$, even though the k_{off} for $mNa_V1.6$ was 17-fold larger than that for $rNa_V1.2$ (Table 2 and Figure 4).

Block of $rNa_V1.5$ and $rNa_V1.2$[C385C] Induced by Reaction with MTSET Is Slowly Reversible. As mentioned in the introductory section, $Na_V1.5$ has a Cys residue with a free thiol that is susceptible to reaction with methanethiosulfonate (MTS) analogues. Thus, for example, reaction of MTSET with human $Na_V1.5$ ($hNa_V1.5$) results in an ET (also known as thiocholine) disulfide-bonded to Cys 373, which is near the ion selectivity filter and site 1 of the pore loop of domain 1 (see Figure S1 of the Supporting Information), that drastically reduces the channel's Na^+ conductance.[5] We performed essentially the same experiment with $rNa_V1.5$, which like $hNa_V1.5$ has a Cys in domain I near the selectivity filter (see Figure S1 of the Supporting Information). As expected, exposure to MTSET blocked I_{Na}; moreover, the block was slowly reversed following washout of MTSET (Figure 5A).

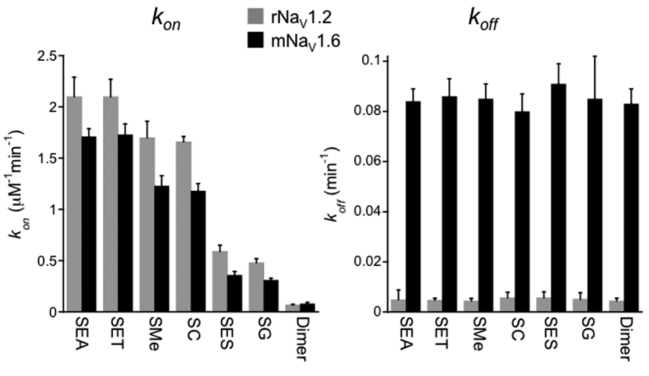

Figure 4. For a given Na_V1 isoform, μO§-$GVIIJ_{SSR}$ derivatives with different SR groups have different k_{on} values but the same k_{off}. Bar graphs of k_{on} (left) and k_{off} (right) for the block of $rNa_V1.2$ (gray) and $mNa_V1.6$ (black) by seven $GVIIJ_{SSR}$'s, where the SR group is indicated on the *x*-axis. Data are means ± SD ($N \geq 3$ oocytes). Derivatives with different SRs had a broad range of k_{on} values (left), but for a given Na_V1 isoform, all derivatives had essentially the same k_{off} value ($p > 0.05$) (right). These results (but in numerical form) are listed in Table 2, which also illustrates the chemical structures of the SR groups.

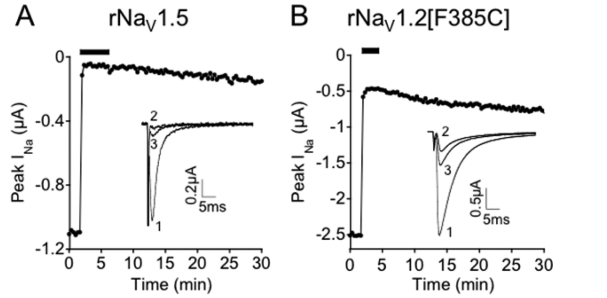

Figure 5. Block of $rNa_V1.5$ and $rNa_V1.2$[F385C] by MTSET treatment is slowly reversible. Oocytes were voltage clamped essentially as described in the legend of Figure 3 and exposed to 2 mM MTSET as described in Materials and Methods. (A and B) Representative time courses of block and recovery of peak I_{Na} values of (A) $rNa_V1.5$ and (B) $rNa_V1.2$[F385C] during exposure to MTSET (black bar) followed by continuous washing. The inset in each panel shows representative traces before treatment (trace 1), after exposure to MTSET for ~5 min (trace 2), and after washing for ~25 min (trace 3). The k_{off} values for the recovery from block following washout of MTSET were 0.004 ± 0.0008 and 0.0111 ± 0.0036 min^{-1} ($N \geq 4$) for $rNa_V1.5$ and $rNa_V1.2$[F385C], respectively.

Experiments with $rNa_V1.2$[F385C], a mutant with a Cys replacing Phe at the location homologous to the Cys in human and rat $Na_V1.5$ (see Table S1 of the Supporting Information), yielded similar results; that is, the block induced by MTSET treatment was slowly reversible (Figure 5B).

Comparison of the Reversibilities of the Block of Cysteine Replacement Mutants of $Na_V1.2$ by $GVIIJ_{SSG}$ and $GVIIJ_{SH}$. Representative time courses for the block by $GVIIJ_{SSG}$ and $GVIIJ_{SH}$ of WT $rNa_V1.2$, $rNa_V1.2$[C912A], and $rNa_V1.2$[C918A], all without and with DTT pretreatment of oocytes, are illustrated in Figure 6. The most distinctive features among these plots are the differences in the kinetics of recovery from toxin block, which are listed in Table 3. DTT treatment of

DOI: 10.1021/acs.biochem.5b00390
Biochemistry 2015, 54, 3911−3920

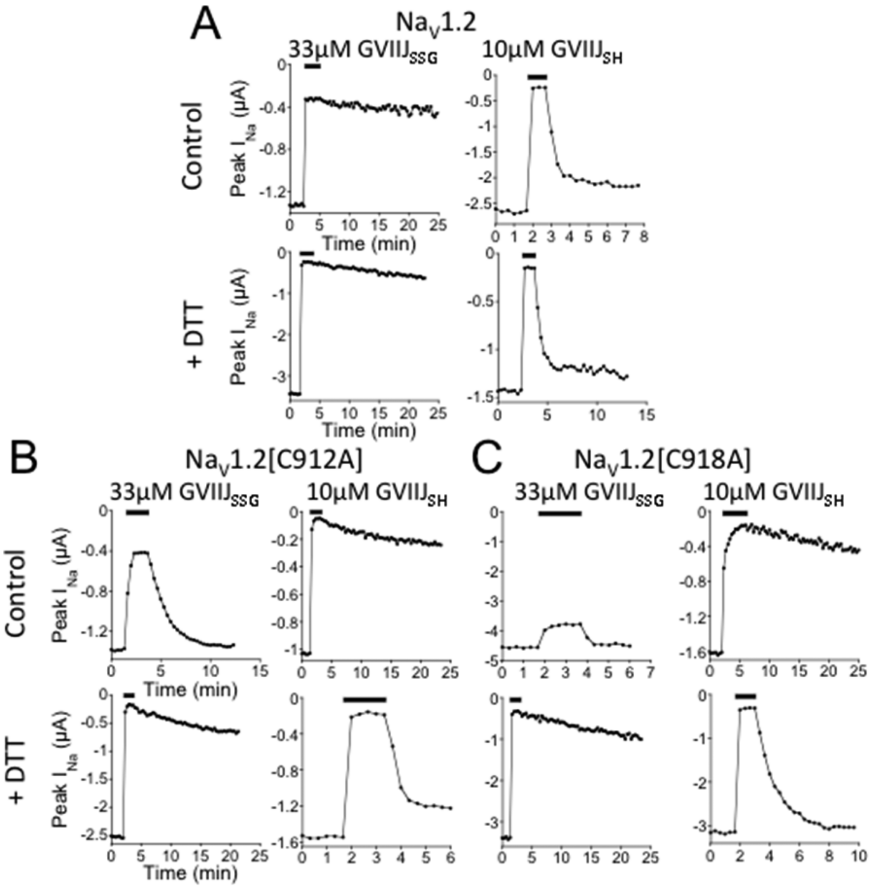

Figure 6. Representative time courses of block by GVIIJ$_{SSG}$ or GVIIJ$_{SH}$ of WT and three Cys replacement mutants of rNa$_V$1.2 in oocytes without and with DTT treatment. Oocyte recordings were conducted as described in the legend of Figure 3. In each panel of four plots, the block by 33 μM GVIIJ$_{SSG}$ is shown in the left pair and that by 10 μM GVIIJ$_{SH}$ is the right pair; the upper pair is of control oocytes and the lower pair of DTT-treated oocytes. These are saturating concentrations of peptide (cf. ref 9) [except for GVIIJ$_{SSG}$ on rNa$_V$1.2[C910A] where higher concentrations yielded greater block (not illustrated)] to obtain the maximal levels of block listed in Table 3. For WT Na$_V$1.2, recovery from block by GVIIJ$_{SSG}$ was slow and that by GVIIJ$_{SH}$ was fast; furthermore, DTT treatment had no effects except to increase the level of block by GVIIJ$_{SSG}$ (A). For both mutants, rNa$_V$1.2[C912A] (B) and rNa$_V$1.2[C918A] (C), in control oocytes recovery from block by GVIIJ$_{SSG}$ was fast while that by GVII$_{SH}$ was slow; conversely, in DTT treated oocytes, recovery from block by GVIIJ$_{SSG}$ was slow while that from block by GVIIJ$_{SH}$ fast. The level of block by GVIIJ$_{SSG}$ was higher in DTT-treated oocytes than in control oocytes in all panels. Values of k_{off} (and percentage block) from replicate trials are listed in Table 3.

Table 3. Values of k_{off} and Percentage Block for the Inhibition by GVIIJ$_{SSG}$ and GVIIJ$_{SH}$ of WT rNa$_V$1.2, rNa$_V$1.2[C912A], and rNa$_V$1.2[C918A], and Their Modification by DTT Treatment of Oocytes[a]

peptide	pretreatment	WT rNa$_V$1.2	rNa$_V$1.2[C912A]	rNa$_V$1.2[C918A]
GVIIJ$_{SSG}$	none	0.0051 ± 0.0026[b,c] (73 ± 10%)	0.39 ± 0.08 (73 ± 11%)	3.17 ± 1.01 (20 ± 3%)
	DTT[d]	0.0055 ± 0.0010[c,e] (89 ± 3%)	0.0084 ± 0.0015[e] (89 ± 3%)	0.0083 ± 0.0014[e] (90 ± 2%)
GVIIJ$_{SH}$	none	2.0 ± 0.2[f,g] (88 ± 4%)	0.009 ± 0.0008[g] (92 ± 4%)	0.01 ± 0.002[g] (88 ± 2%)
	DTT[d]	1.93 ± 0.19[f,h] (89 ± 3%)	2.20 ± 0.26[h] (88 ± 2%)	1.22 ± 0.47[h] (90 ± 2%)

[a]Values of k_{off} (in min^{-1}) and percentage block (in parentheses) are means ± SD ($N \geq 3$); concentrations of peptides used to obtain percentage block are those shown in Figure 6. [b]From Table 1. [c]Values for WT with or without DTT treatment do not differ ($p > 0.7$). [d]Oocytes were treated with DTT as described in Materials and Methods. [e]Values for mutants do not differ from each other ($p > 0.9$) and differed only marginally, if at all, from that of WT ($p = 0.05$). [f]Values for WT with or without DTT treatment do not differ ($p > 0.7$). [g]Values for mutants do not differ from each other ($p > 0.3$) but differ from that of WT ($p < 0.001$). [h]Values for mutants marginally differed from each other ($p = 0.05$), and neither differed from that of WT ($p > 0.1$).

oocytes expressing WT rNa$_V$1.2 did not significantly alter the time course of recovery from block by either peptide, which was slow for GVIIJ$_{SSG}$ and fast for GVIIJ$_{SH}$. In contrast, the recovery from block by GVIIJ$_{SSR}$ and GVIIJ$_{SH}$ for both rNa$_V$1.2[C912A] and rNa$_V$1.2[C918A] was fast and slow, respectively. Furthermore, DTT treatment of the oocytes inverted the reversibilities of the block by GVIIJ$_{SSG}$ and GVIIJ$_{SH}$ (Figure 6 and Table 3). In other words, for both mutants in control oocytes, the block by GVIIJ$_{SSG}$ was rapidly reversible whereas that by GVIIJ$_{SH}$ was slowly reversible, and the converse was observed with DTT-treated oocytes: the block by GVIIJ$_{SSG}$ was slowly reversible, and that by GVIIJ$_{SH}$ was rapidly reversible.

DOI: 10.1021/acs.biochem.5b00390
Biochemistry 2015, 54, 3911−3920

DISCUSSION

Only two reports regarding GVIIJ have appeared thus far. The first report characterized the discovery and structure of GVIIJ and examined the effects of three derivatives ($GVIIJ_{SSG}$, $GVIIJ_{SSC}$, and $GVIIJ_{SH}$) on exogenously expressed channels,[9] while the second report characterized the effects of $GVIIJ_{SSG}$ and $GVIIJ_{SSC}$ on (endogenously expressed) channels in neurons.[19] In the report presented here, we used exogenously expressed channels to examine the mechanism by which GVIIJ interacts with the channel.

Seven $GVIIJ_{SSR}$ Derivatives Block $rNa_V1.2$ and $mNa_V1.6$ with Variable On Rates, but All Have the Same Off Rate for a Given Na_V1 Isoform. We previously reported that the k_{off} values of the six Na_V1 isoforms that were highly susceptible to $GVIIJ_{SSG}$ (namely, $rNa_V1.1$, $rNa_V1.2$, $rNa_V1.3$, $rNa_V1.4$, $rNa_V1.6$, and $rNa_V1.7$) were all rather similar ($\leq$0.005 min^{-1}) except that of $rNa_V1.6$, for which the k_{off} was 0.12 ± 0.016 min^{-1} (Table S3 of ref 9). The latter value is close to that for $mNa_V1.6$, 0.085 ± 0.017 min^{-1} (Table 2). A total of seven $GVIIJ_{SSR}$ derivatives were tested for their kinetics of block of $rNa_V1.2$ and $mNa_V1.6$, and although their k_{on} values ranged over more than 1 order of magnitude, their k_{off} values were statistically the same (Table 2 and Figure 4). These results support the hypothesis that binding of $GVIIJ_{SSR}$ to the channel involves a disulfide bond formed by disulfide exchange. Thus, Figure 1C illustrates what we believe to be the most parsimonious reaction mechanism consistent with all of our results.

The functional activity of the dimer seems remarkable and deserves comment. The fact that its on rate is slower than those of any of the other $GVIIJ_{SSR}$ derivatives (Table 2) is not surprising given its larger mass. The fact that the dimer is otherwise quite active suggests that Cys910 (using $rNa_V1.2$ numbering) of the channel is likely to be sterically quite accessible. In other words, it is possible that the free thiol of Cys910 protrudes sufficiently from the channel's surface at site 8, and the area immediately surrounding it is sufficiently uncrowded that the disulfide bond linking the two monomers of the dimer can interact with the thiol of Cys910. Reciprocally, the disulfide bond linking the two monomers of the dimer must be accessible for disulfide exchange with Cys910 of the channel. Consistent with the latter is the observation that the dimer's disulfide bond was reduced by TCEP at a rate comparable with those of disulfide bonds between peptide and SR groups where R was SG, SEA, and SC (not illustrated, but cf. Figure 2B), a result consonant with the notion that the disulfide bridge between the monomers of the dimer is sterically readily accessible.

Experiments Examining the Reversibility of the Disulfide Bond between Thiocholine and a Cysteine Residue near Site 1 of $rNa_V1.5$ and $rNa_V1.2$[F385C]. The disulfide bond, although covalent, can be labile under physiological conditions depending on the residues in its immediate environment.[24] Because this phenomenon may not be widely appreciated, we examined the disulfide bond between thiocholine and a Cys residue of $rNa_V1.5$ and $rNa_V1.2$[F385C] whose stability could be conveniently monitored electrophysiologically. Previous experiments by others showed that the sodium ion permeability of $hNa_V1.5$ (but not that of the mutant $hNa_V1.5$[C373Y]) was blocked by treatment with the membrane-impermeant reagent MTSET.[5] We reproduced this experiment with $rNa_V1.5$ and furthermore observed that the block was slowly reversed following washout of MTSET (Figure 5A). The block induced by MTSET treatment of $rNa_V1.2$[F385C] was also reversible (Figure 5B). (Note, WT $Na_V1.2$ is not blocked by MTSET treatment.[9]) We presume that the recovery of sodium current reflects the lability of the S−S bond between the channel cysteine and thiocholine. These results lend support to the reversible nature of the hypothesized disulfide bond between Cys24 of GVIIJ and the Cys residue at site 8 of the channel (Figure 1C).

Block of Cysteine Replacement Mutant Channels without and with DTT Treatment by $GVIIJ_{SSG}$ and $GVIIJ_{SH}$. Among the 13 absolutely conserved Cys residues illustrated in Figure 1B, all but the three are also present in $rNa_V1.5$ and $rNa_V1.8$ (see Table S1 of the Supporting Information), which $GVIIJ_{SSG}$ blocks poorly and not at all, respectively.[9] For $rNa_V1.2$, those three cysteines are at positions 910, 912, and 918. As described in the introductory section, we previously showed the importance of the first of these cysteines by its "knockout" from $rNa_V1.2$ and conversely its "knock-in" into $rNa_V1.5$, which essentially produced loss-of-susceptibility and gain-of-susceptibility mutants, respectively.[9] Here, we examined the roles of the second and third cysteines in $rNa_V1.2$ with mutants lacking either of these residues and testing with $GVIIJ_{SSG}$ and $GVIIJ_{SH}$.

As previously reported,[9] the block of wild-type $rNa_V1.2$ by $GVIIJ_{SSG}$ was slowly reversible, while that by $GVIIJ_{SH}$ was rapidly reversible; furthermore, treatment of oocytes with DTT did not alter the kinetics (Figure 6A and Table 3). In stark contrast, the block of both $rNa_V1.2$[C912A] and $rNa_V1.2$[C918A] by $GVIIJ_{SSR}$ was rapidly reversible, while that by $GVIIJ_{SH}$ was slowly reversible. Furthermore, when oocytes expressing these mutant channels were pretreated with DTT, the inverse results were observed; that is, the reversibility of block by $GVIIJ_{SSG}$ was slow and that by $GVIIJ_{SH}$ fast (Figure 6B,C and Table 3). A reaction scheme consistent with these data is presented in the cartoon of Figure 7, which shows Cys910 disulfide-bonded to Cys918 in $rNa_V1.2$[C912A] (Figure 7A) and to Cys912 in $rNa_V1.2$[C918A] (Figure 7A′).

In this regard, it might be noted that treatment of $rNa_V1.2$-expressing oocytes with MTSET protects against block by $GVIIJ_{SSG}$ but not by $GVIIJ_{SH}$; on the contrary, MTSET treatment converts the normally rapidly reversible block by $GVIIJ_{SH}$ to one that is only slowly reversible (like that of $GVIIJ_{SSG}$ under normal conditions).[9] These observations are consistent with the scheme in Figure 7. (Note that Figure 7 is a derivative of Figure 3C of ref 9, which summarized the results of that report, including the observations with MTSET.) The GVIIJ derivatives used in this report involved alterations solely to Cys24 of the peptide. Also of interest are derivatives in which residues in the peptide backbone are altered. Experiments with such GVIIJ derivatives are in progress (B. R. Green et al., manuscript in preparation).

Comparison of Results of Oocytes with Those of Neurons. We have performed tests with $GVIIJ_{SSG}$ on patch-clamped dissociated DRG neurons from rat and observed that the tetrodotoxin-sensitive (TTX-s) I_{Na} values of small (but not large) neurons were sensitive to 10 μM $GVIIJ_{SSG}$; furthermore, the TTX-s I_{Na} was incompletely blocked.[19] There are at least two possible explanations for the incomplete block. (1) A fraction of the Na_V1s may be co-expressed with $Na_V\beta2$ or $\beta4$ subunits, which in oocytes prevents $GVIIJ_{SSG}$ block.[9,19] (2) $GVIIJ_{SSG}$ produces an incomplete block just as in oocytes. We have yet to examine whether DTT treatment reduces the

DOI: 10.1021/acs.biochem.5b00390
Biochemistry 2015, 54, 3911−3920

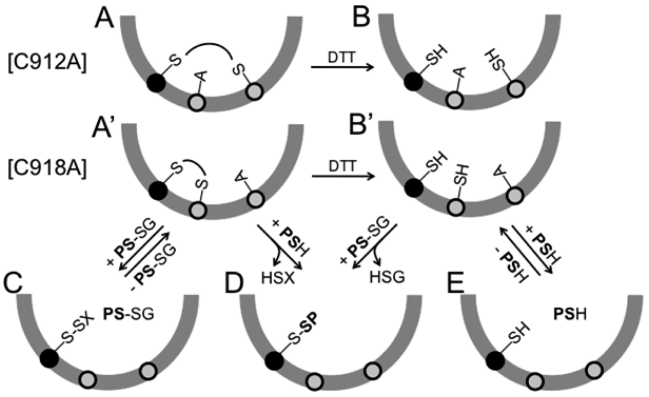

Figure 7. Sketch of proposed redox states of cysteine residues at site 8 in $rNa_V1.2$[C912A] and $rNa_V1.2$[C918A] before and after DTT treatment of oocytes. The filled circle represents Cys910. The gray circles represent the locations of residues 912 and 918, which are cysteines (indicated by "-S-" or "-SH") or alanines (indicated by "-A") in the mutants. (A–E) Reaction scheme before and after reduction with DTT (A or A′ and B or B′, respectively). The SX moiety represents a channel cysteine. The solid arcs in parts A and A′ represent proposed disulfide bonds between Cys910 and Cys918 (in A) and between Cys910 and Cys912 (in A′). Channels at the left (A and A′) react reversibly with $GVIIJ_{SSG}$ to form C but "irreversibly" with $GVIIJ_{SH}$ to form D (where the peptide is disulfide-tethered to Cys910). Conversely, channels after DTT treatment (B and B′) react "irreversibly" with $GVIIJ_{SSG}$ to form D but reversibly with $GVIIJ_{SH}$ to form E.

incomplete block of neuronal currents as it does the currents of channels expressed in oocytes.

Unresolved Issues. The reason why the k_{off} of $GVIIJ_{SSG}$ (or $GVIIJ_{SSR}$ in general) is larger for rat and mouse $Na_V1.6$ than for $rNa_V1.2$ and other rNa_V1 isoforms is unknown. This issue may be resolved by investigating domain-swapped chimeras of $Na_V1.6$ and $Na_V1.2$ (e.g., as was done with $hNa_V1.5$ and $hNa_V1.7$[9]). Another unresolved issue is that in untreated oocytes, the block of WT $rNa_V1.2$ by saturating concentrations of $GVIIJ_{SSG}$ is 70%, which increases to 90% following DTT treatment; in contrast, maximal block by $GVIIJ_{SH}$ is 90% regardless of whether the oocyte is DTT-treated.[9] These features are also evident in Figure 6A and Table 3. From the percentage block values in Table 3, it appears that the channel's state in Figure 7C corresponds to ∼70% block while states in panels D and E of Figure 7 correspond to ∼90% block. A perhaps related unresolved issue is that we do not yet understand how GVIIJ blocks the channel, although mechanisms for both of these issues have been proposed.[9]

An intriguing observation is that co-expression of $Na_V\beta2$ or $Na_V\beta4$ (but not that of $Na_V\beta1$ or $Na_V\beta3$) with $rNa_V1.1$–1.4, $rNa_V1.6$, or $rNa_V1.7$ protects against block by $GVIIJ_{SSG}$.[9,19] As mentioned in the introductory section, $Na_V\beta2$ and $Na_V\beta4$ (but neither $Na_V\beta1$ nor $Na_V\beta3$) are disulfide-bonded to the α-subunit.[7,8] Which Cys in the α-subunit can be disulfide-bonded to $Na_V\beta2$ or $\beta4$ remains to be established, but in view of the interaction of $GVIIJ_{SSG}$ with site 8, it was suggested that Cys910 (using $Na_V1.2$ numbering) might be culpable.[9] Channel purification and mass spectrometry may be the final arbiter here as well as in (1) confirming that a disulfide bond is formed between GVIIJ and the channel and (2) establishing the redox states of the other Cys residues illustrated in Figure 1B.

Conclusions. Extracellular cysteine residues are found exclusively in the loop between S5 and S6 in all domains of all Na_V1 isoforms from rat and human; furthermore, 11 of these are conserved in essentially all isoforms, and an additional three are conserved in each of the six GVIIJ-susceptible isoforms from both rat and human (Figure 1B and Table S1 of the Supporting Information). The conservation of these residues is a strong indicator that they serve important roles. The redox states of these extracellular cysteines are largely unexplored areas into which synthetic derivatives of GVIIJ afford a unique peek. In addition, an appreciation of the results with GVIIJ derivatives (and maleimide conjugates of saxitoxin[6]) raises awareness that extracellular cysteines of sodium channels could be exploited in targeting or tethering drugs to these channels.

■ ASSOCIATED CONTENT

Supporting Information

Aligned sequences in the loop between S5 and S6 in domains I–IV of $Na_V1.1$–1.9 from rat and human, which illustrate the highly conserved locations of extracellular Cys residues, and mass spectra of $GVIIJ_{SSEA}$, $GVIIJ_{SSET}$, $GVIIJ_{SSMe}$, $GVIIJ_{SSES}$, and $(GVIIJ_S)_2$. The Supporting Information is available free of charge on the ACS Publications website at DOI: 10.1021/acs.biochem.5b00390.

■ AUTHOR INFORMATION

Corresponding Author

*Department of Biology, University of Utah, 257 S. 1400 East, Salt Lake City, UT. E-mail: yoshikami@bioscience.utah.edu. Telephone: (801) 581-3084. Fax: (801) 328-4668.

Author Contributions

J.G. and L.A. contributed equally to this work.

Funding

This work was supported by National Institutes of Health Grant GM 48677. Peptide syntheses were also supported in part by funds from Janssen Research and Development, LLC.

Notes

The authors declare no competing financial interest.

■ ACKNOWLEDGMENTS

We thank Prof. Alan A. Goldin (University of California, Irvine, CA) for the clones of $rNa_V1.2$ and $mNa_V1.6$ and William Low for performing peptide mass spectrometry at the facilities of The Salk Institute for Biological Studies (La Jolla, CA). We also thank Dr. Aleksandra Walewska and Brad R. Green for helpful discussion regarding peptide synthesis and characterization and Drs. Helena Safavi-Hemami and Beatrix Ueberheide for help interpreting mass spectra.

■ ABBREVIATIONS

DTT, dithiothreitol; GVIIJ, μO§-conotoxin GVIIJ from *Conus geographus*; $GVIIJ_{SH}$, synthetic GVIIJ with Cys24 having a free thiol; $GVIIJ_{SSR}$, synthetic GVIIJ with Cys24 derivatized with different SR groups listed in Table 2; I_{Na}, sodium current; MTSET, [2-(trimethylammonium)ethyl]methanethiosulfonate; Na_V1, α-subunit of VGSC; $Na_V\beta$, β-subunit of VGSC; VGSC, voltage-gated sodium channel.

■ REFERENCES

(1) Catterall, W. A. (2012) Voltage-gated sodium channels at 60: Structure, function and pathophysiology. *J. Physiol. (Oxford, U.K.) 590*, 2577–2589.

DOI: 10.1021/acs.biochem.5b00390
Biochemistry 2015, 54, 3911–3920

(2) Calhoun, J. D., and Isom, L. L. (2014) The Role of Non-pore-Forming β Subunits in Physiology and Pathophysiology of Voltage-Gated Sodium Channels. *Handb. Exp. Pharmacol. 221*, 51−89.
(3) Brackenbury, W. J., and Isom, L. L. (2011) Na Channel β Subunits: Overachievers of the Ion Channel Family. *Front. Pharmacol. 2*, 53.
(4) O'Malley, H. A., and Isom, L. L. (2015) Sodium Channel β Subunits: Emerging Targets in Channelopathies. *Annu. Rev. Physiol. 77*, 481−504.
(5) Kirsch, G. E., Alam, M., and Hartmann, H. A. (1994) Differential effects of sulfhydryl reagents on saxitoxin and tetrodotoxin block of voltage-dependent Na channels. *Biophys. J. 67*, 2305−2315.
(6) Parsons, W. H., and Du Bois, J. (2013) Maleimide Conjugates of Saxitoxin as Covalent Inhibitors of Voltage-Gated Sodium Channels. *J. Am. Chem. Soc. 135*, 10582−10585.
(7) Chen, C., Calhoun, J. D., Zhang, Y., Lopez-Santiago, L., Zhou, N., Davis, T. H., Salzer, J. L., and Isom, L. L. (2012) Identification of the cysteine residue responsible for disulfide linkage of Na^+ channel α and β2 subunits. *J. Biol. Chem. 287*, 39061−39069.
(8) Gilchrist, J., Das, S., Van Petegem, F., and Bosmans, F. (2013) Crystallographic insights into sodium-channel modulation by the β4 subunit. *Proc. Natl. Acad. Sci. U.S.A. 110*, E5016−E5024.
(9) Gajewiak, J., Azam, L., Imperial, J., Walewska, A., Green, B. R., Bandyopadhyay, P. K., Raghuraman, S., Ueberheide, B., Bern, M., Zhou, H. M., Minassian, N. A., Hagan, R. H., Flinspach, M., Liu, Y., Bulaj, G., Wickenden, A. D., Olivera, B. M., Yoshikami, D., and Zhang, M.-M. (2014) A disulfide tether stabilizes the block of sodium channels by the conotoxin μO§-GVIIJ. *Proc. Natl. Acad. Sci. U.S.A. 111*, 2758−2763.
(10) Cestèle, S., and Catterall, W. A. (2000) Molecular mechanisms of neurotoxin action on voltage-gated sodium channels. *Biochimie 82*, 883−892.
(11) Leipold, E., DeBie, H., Zorn, S., Borges, A., Olivera, B. M., Terlau, H., and Heinemann, S. H. (2007) muO conotoxins inhibit NaV channels by interfering with their voltage sensors in domain-2. *Channels 1*, 253−262.
(12) Kenyon, G. L., and Bruice, T. W. (1977) Novel sulfhydryl reagents. *Methods Enzymol. 47*, 407−430.
(13) Akabas, M. H., Stauffer, D. A., Xu, M., and Karlin, A. (1992) Acetylcholine receptor channel structure probed in cysteine-substitution mutants. *Science 258*, 307−310.
(14) Akaji, K., and Kiso, Y. (2002) Synthesis of Peptides and Peptidomimetics. In *Houben-Weyl, Methods of Organic Chemistry* (Goodman, M., Felix, A., Moroder, L., and Toniolo, C., Eds.) pp 101−141, Thieme, Stuttgart, Germany.
(15) Zhang, M.-M., McArthur, J. R., Azam, L., Bulaj, G., Olivera, B. M., French, R. J., and Yoshikami, D. (2009) Synergistic and antagonistic interactions between tetrodotoxin and μ-conotoxin in blocking voltage-gated sodium channels. *Channels 3*, 32−38.
(16) Cartier, G. E., Yoshikami, D., Gray, W. R., Luo, S., Olivera, B. M., and McIntosh, J. M. (1996) A new α-conotoxin which targets α3β2 nicotinic acetylcholine receptors. *J. Biol. Chem. 271*, 7522−7528.
(17) Zhang, M. M., Wilson, M. J., Azam, L., Gajewiak, J., Rivier, J. E., Bulaj, G., Olivera, B. M., and Yoshikami, D. (2013) Co-expression of Na(V)β subunits alters the kinetics of inhibition of voltage-gated sodium channels by pore-blocking μ-conotoxins. *Br. J. Pharmacol. 168*, 1597−1610.
(18) Wilson, M. J., Yoshikami, D., Azam, L., Gajewiak, J., Olivera, B. M., Bulaj, G., and Zhang, M. M. (2011) μ-Conotoxins that differentially block sodium channels NaV1.1 through 1.8 identify those responsible for action potentials in sciatic nerve. *Proc. Natl. Acad. Sci. U.S.A. 108*, 10302−10307.
(19) Wilson, M. J., Zhang, M.-M., Gajewiak, J., Azam, L., Rivier, J. E. F., Olivera, B. M., and Yoshikami, D. (2015) α- and β-Subunit Composition of Voltage-gated Sodium Channels Investigated with μ-Conotoxins and the Recently Discovered μO§-Conotoxin GVIIJ. *J. Neurophysiol. 113*, 2289−2301.
(20) Hille, B. (2001) *Ion Channels in Excitable Membranes*, 3rd ed., p 505, Sinauer Associates, Sunderland, MA.
(21) West, P. J., Bulaj, G., Garrett, J. E., Olivera, B. M., and Yoshikami, D. (2002) μ-Conotoxin SmIIIA, a potent inhibitor of tetrodotoxin-resistant sodium channels in amphibian sympathetic and sensory neurons. *Biochemistry 41*, 15388−15393.
(22) Wilson, M. J., Zhang, M. M., Azam, L., Olivera, B. M., Bulaj, G., and Yoshikami, D. (2011) Navβ subunits modulate the inhibition of Nav1.8 by the analgesic gating modifier μO-conotoxin MrVIB. *J. Pharmacol. Exp. Ther. 338*, 687−693.
(23) Kuang, Z., Zhang, M.-M., Gupta, K., Gajewiak, J., Gulyas, J., Balaram, P., Rivier, J. E., Olivera, B. M., Yoshikami, D., Bulaj, G., and Norton, R. S. (2013) Mammalian neuronal sodium channel blocker μ-conotoxin BuIIIB has a structured N-terminus that influences potency. *ACS Chem. Biol. 8*, 1344−1351.
(24) Goldenberg, D. P., Bekeart, L. S., Laheru, D. A., and Zhou, J. D. (1993) Probing the determinants of disulfide stability in native pancreatic trypsin inhibitor. *Biochemistry 32*, 2835−2844.
(25) Catterall, W. A., Goldin, A. L., and Waxman, S. G. (2005) International Union of Pharmacology. XLVII. Nomenclature and structure-function relationships of voltage-gated sodium channels. *Pharmacol. Rev. 57*, 397−409.

DOI: 10.1021/acs.biochem.5b00390
Biochemistry 2015, 54, 3911−3920